Catalytic properties of 3D graphene-like microporous carbons synthesized in a zeolite template

Petr Sazama,[*1] Jana Pastvova,[1,6] Jiri Rathousky,[1] *Cristina Rizescu,[2] Alina Tirsoaga,[2]Vasile I. Parvulescu,[2]* Libor Kobera,[4] Petr Klein,[1] Ivan Jirka,[1]Nemec,[5] *Hermenegildo Garcia,[7n]*Vaclav Blechta,[1]

[1]*J. Heyrovský Institute of Physical Chemistry, Academy of Sciences of the Czech Republic, CZ-182 23 Prague 8, Czech Republic, Email:*

[2]*University of Bucharest, Department of Organic Chemistry and Catalysis, B-dul Regina Elisabeta 4-12, 030016 Bucharest, Romania*

[3]*Instituto Universitario de Tecnología Química (CSIC-UPV) and Department of Chemistry (UPV), Av. de los Naranjos S/N, 46022, Valencia, Spain*

[4]*Institute of Macromolecular Chemistry, Academy of Sciences of the Czech Republic, Heyrovsky sq. 2, 162 06 Prague 6, Czech Republic*

[5]*Institut für Physikalische Chemie, TU Bergakademie Freiberg, Leipziger Str. 29, 09596 Freiberg/Sachsen, Germany*

[6]*University of Pardubice, Studentska 95, Pardubice, 532 10, Czech Republic*

[7]*Instituto de Tecnología Química CSIC-UPV, Universitat Politecnica de Valencia, Av. de los Naranjos s/n, 46022 Valencia, Spain*

Abstract

The inherent properties of a single atomic carbon layer in graphene offer new opportunities for the creation of catalytically active centers tailored on a molecular level on a support with high thermal stability, as well as outstanding mechanical properties and specific surface area. We demonstrate that organization of the two-dimensional system of the carbon layer into three-dimensional (3D) graphene-like catalytic materials with connectivity of a pore network providing good accessibility to the active centres allows the preparation of a conceptually new class of catalytic materials exploiting graphene properties. In this study, 3D graphene-like microporous carbons, denoted as β-graphene and Y-graphene, were synthesized by nanocasting of beta (*BEA) and faujasite (FAU) zeolite templates. Structural analyses show that the materials are characterised by 3D assembled and highly stable single atomic graphene layers forming an open porous system resembling the regular channel system of the zeolites with a specific surface area comparable to the surface area of graphene. The materials effectively catalyse the hydrogenation of alkenes, alkynes and cycloalkenes into the corresponding alkanes and cycloalkanes. The materials facilitate catalytic intramolecular rearrangements including the selective isomerisation of double bonds and branching of linear chains, as well as stereo-selective isomerisation of unsaturated hydrocarbons.

The large surface area (~2630 m^2.g^{-1}), thermal stability, and wide range of means of functionalizing the graphene monolayer[1-6] could be exploited in the development of a conceptually new class of heterogeneous catalysts with active sites controlled at the atomic level. Oxygen-containing functional groups, the unsaturated carbon atoms at the edges of one-atom-thick graphene, or metal and metal-oxide nanoparticles of defined structures grafted onto graphene exhibit high catalytic activity for oxidation, reduction and coupling reactions.[7-11] However, utilization of the unique properties of graphene for application in a catalytic process relies on the development of a three-dimensional (3D) graphene-like catalytic material with connectivity of the pore network, providing good accessibility to the active centres. The gas-impermeable layers of graphene limit the use of graphene sheets assembled into 3D structures, imposing limitations on the mass transport of reactant molecules to and from the active sites in microscopic catalysts. Typically, the total surface area of single-wall nanotubes (SWNT) and multi-wall carbon nanotubes (MWNT) ranges between only 200 and 400 m^2.g^{-1} and 400 and 900 m^2.g^{-1}, respectively[12].

Recently, the structure of 3D graphene-like architectures with periodic nanopores synthesized by nanocasting of zeolitic structures was described by Ryoo et.al.[13] Zeolites as crystalline alumosilicates with well-defined and regular 3D channels can be replicated into the carbon materials with well-defined dimensions and spatial connectivity of the micropores.[14-16] In the process of zeolite nanocasting, carbon atoms are generated along the walls of the regular zeolite micropores[13] and subsequent selective removal of the structural lattice of the zeolite provides an ordered 3D microporous graphene-like carbon material. The defined size of the zeolite channels in the range from 0.3 to 1.5 nm and ordered arrangement of pores characteristic of particular structural topologies enable the formation of carbon materials with well-controlled porosity on the sub-nanometer scale. The ultra-high surface area, narrow pore-size distribution and specific morphology of these carbon materials provided an exceptional potential for controlling the functionality in numerous applications in the areas of energy and gas storage.[17-24]

In this study, 3D graphene-like microporous carbons synthesized in the beta (*BEA) and faujasite (FAU) zeolite templates, denoted as β-graphene and Y-graphene, respectively, were analysed with respect to their structure and catalytic properties in comparison with conventional graphene and few-layer graphene sheet materials. Their structural and textural properties were investigated using XRD, SEM, TEM and adsorption of N$_2$, the coordination of carbon atoms and the presence of defective sites and functional groups by complementary XPS, Raman, and ^{13}C MAS NMR spectroscopies. Their thermal stability was determined using

thermogravimetric analysis (TGA) coupled with differential scanning calorimetry (DSC). The functionality of β-graphene and Y-graphene carbons is demonstrated on a series of catalytic hydro-transformations of alkenes, alkynes and cycloalkenes.

Results and Discussion

Structure of 3D graphene-like zeolite templated carbons

The X-ray powder diffractogram of β-graphene in figure 1a is characterised by intense signals at 8 and 14° 2θ, reflecting the spacing between the basal diffraction planes given by the replication of the centrosymmetrical tertiary building units of the *BEA zeolite template ($a\sim1.2$ nm)[25,26] and close spatial arrangement of the carbon material and zeolite pores,[20] showing a high level of replication of the zeolite-type structural ordering in β-graphene. Similarly for Y-graphene, the diffraction peak at 6° 2θ reflects the replication of the planes of the Y zeolite crystal. The very low intensity of the broad diffraction lines at 24° 2θ corresponding to the (002) reflection characteristic of layered multiple graphene sheets is consistent with negligible stacking of graphene sheets forming graphitic platelets and the appearance of the peak at 42° 2θ corresponds to the (100) reflection of the planar aromatic lattice of graphene, indicating large lateral dimensions of the graphene sheets. The surface areas of 2454 and 2443 $m^2.g^{-1}$ for β-graphene and Y-graphene (figure 1b), respectively, are comparable to the theoretical surface area for graphene of ~2630 $m^2.g^{-1}$ [1] and is much greater compared to the reported surface area of a graphene powder consisting of flexible and curvature sheets resulting in partial stacking, agglomeration and corrugation of the sheets, which normally blocks a significant part of the accessible surface of graphene sheets in powdered samples [1,27]. Ryoo et al.[13] calculated the theoretical pore volume to be 1.45 $cm^3.g^{-1}$ for the faithfully replicated channel structure of the Y zeolite. The pore volume of 1.35 $cm^3.g^{-1}$, predominantly due to micropores 1.25 $cm^3.g^{-1}$, found for Y-graphene indicates a high level of faithful replication of the channel system with a relatively low proportion of partially templated and defective pores, or empty pore regions. SEM images show that the particles of β- and Y-graphene retain the external morphology (Figure S1) of the parent zeolite template and HR-TEM indicates organization of the pores without the formation of stacked graphene layers on the external surface (Figure S2). XPS analysis yielded C1s spectra (Figure 1c) with an identical shape for β-graphene, Y-graphene and ordinary graphene, with a maximum intensity at 284.4 eV characteristic of the sp^2-hybridized carbon atoms with a deformed characteristic angle of 120° between hybrid orbitals forming σ-and π-bonds in the deformed planar graphene layer. The C1s spectra are characterised by low intensity of the bands at 286-290 eV, characteristic of defective centres

and/or oxygen-containing functional groups for all the graphene materials. High-resolution solid state NMR spectra collected with magic angle spinning (MAS) using the very fast (VF) approach and cross-polarization (CP) pulse sequence were employed as the primary method to analyse the coordination of carbon atoms in the prepared materials (Figure 1d). The spectra exhibit characteristic peaks for sp^2-hybridised carbon atoms with maxima at 129.3 and 124.0 ppm, indicating variations in the environments of the sp^2-hybridised carbons in the carbon rings forming the graphene layer. The absence of the signals for hydroxyl and carbonyl groups at about 60 and 188 ppm, respectively, in the ^{13}C VF/MAS NMR spectra and low intensity of the bands in ^{13}C CP/MAS NMR with a selective many-fold enhancement of the signal for these groups indicate their very low concentrations, in agreement with the low intensity of the bands at 286-290 eV in the XPS spectra (Figure 1c). The Raman spectra recorded upon 488 nm excitation for β-graphene and Y-graphene exhibit a much broader and upshifted G band and an intensive D band compared to the bulk graphite and few-layer graphene (Figure 1e). The broadening of the G band, shift of its maximum by about 10 cm^{-1} and the intensity of the D band in the spectra of β-graphene and Y-graphene are compatible with a graphene structure with a large proportion of edges.[28,29] The complex curvature of the graphene sheets forming the 3D channel system along the zeolite walls and rehybridization of the carbon orbital to non-planar sp2 configurations and/or near sp3 hybridization of atoms located at the abundant edges and defects is indicated by the absorption intensity at 1150 and 1500 cm^{-1}.[28,29]. TGA–DSC analysis carried out to compare the thermal stability of graphene-based materials found the combustion points (temperature with the highest rate of mass loss and heat flow) to be 520, 540, 530, and 700 °C for β-graphene, Y-graphene, GO and few-layer graphene, respectively, which indicates sufficient thermal stability for catalytic reactions carried out in a wide range of reaction temperatures. Graphene attack by oxygen should start preferentially at the edges and defects[30] and, therefore, the carbon atoms and GO with intrinsic oxygen defects and populated domain boundaries in β- and Y-graphenes are expected to react with O_2 more easily compared to multilayer graphene.
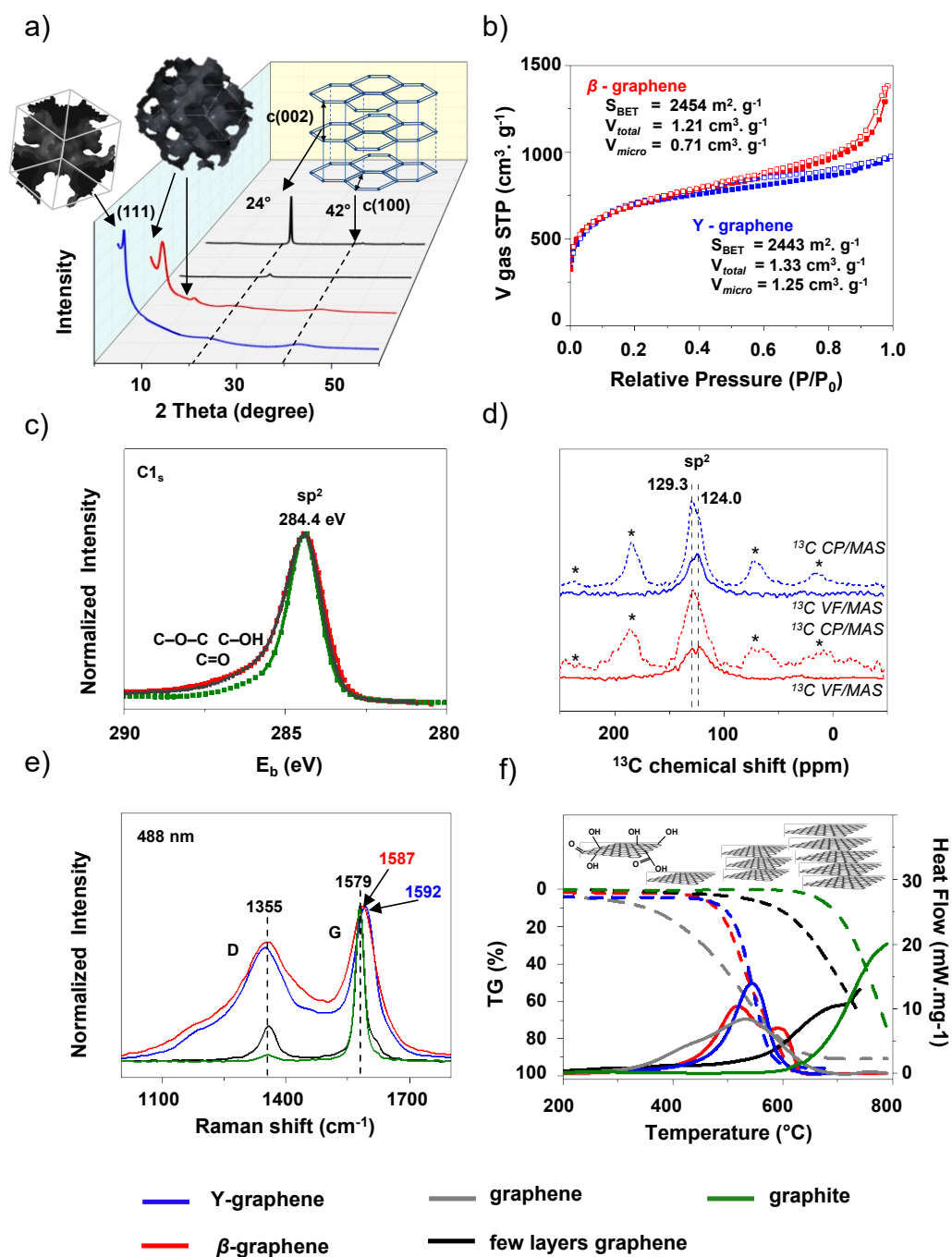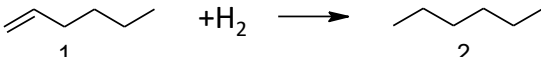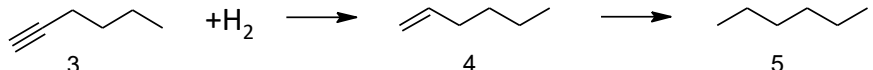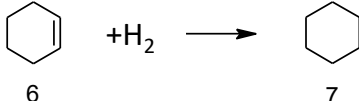
Figure 1. *Characterization of β-graphene and Y-graphene compared with ordinary single and few-layer graphenes. a) X-ray powder diffraction (XRD) patterns with schematic representation of the material structure, b) N₂-sorption isotherms, c) X-ray photoelectron spectroscopy C1s spectra, d) ^{13}C solid state magic-angle-spinning NMR spectra collected using cross-polarization pulse sequence (^{13}C CP/MAS NMR) and the very fast approach (^{13}C VF/MAS NMR), e) Raman spectra upon 488 nm excitation, and f) thermogravimetric analysis (TGA) coupled to differential scanning calorimetry (DSC).*

The structural analysis clearly showed a high level of replication of the zeolite-type structural ordering and porous system into the thermally highly stable carbon materials. The structures of β-graphene and Y-graphene are compatible with sp^2-hybridized carbon atoms in the deformed graphene layer generated along the zeolite walls with negligible formation of layered graphene sheets, a surface area comparable to the theoretical surface area for graphene, high pore volume predominantly represented by micropores and the external morphology of the parent zeolite template.

Catalytic reactions of unsaturated hydrocarbons over β-graphene and Y-graphene

The catalytic behaviour of the β-graphene and Y-graphene was evaluated in the transformation of a series of alkenes (1-hexene, 1-octene, 1-decene), cycloalkenes (cyclohexene, cyclooctene), and alkynes (1-hexyne, 1-phenyl-1-hexyne), (Tables 1, 2 and S1) during hydrogenation reactions. The ability of the 3D-graphene materials to catalyse the hydrogenation of double and triple bonds in linear and cyclic molecules was investigated using 1-hexene, hexyne and cyclohexene (Eq. 1-3 in table I) as model compounds. 1-hexene was selectively hydrogenated to hexane without the production of any products of oligomerization or isomerisation (Table 1). Hydrogenation of 1-hexyne also followed the expected route, where it was hydrogenated to both 1-hexene and hexane, with 1-hexene as the main product. The hydrogenation of cyclohexene selectively yielded cyclohexane with a reaction rate four times higher than the rate of hydrogenation of linear 1-hexene and 1-hexyne. The results indicate that the curved surface of the β-graphene and Y-graphene layers with highly populated edges effectively activate molecules of hydrogen and substrate, promoting hydrogenation of carbon-carbon multiple bonds in the absence of metallic active centres. The energy of hydrogen adsorption on metal clusters is up to one order of magnitude greater[31], but the surface area for hydrogen adsorption on the 3D carbon is three orders of magnitude greater than on a metal catalyst.[32] The comparable rates for the hydrogenation of double and triple carbon-carbon bonds in the linear molecule and significantly increased conversion of the cyclic molecule indicate the important role of the substrate structure (elevctronic and sterivc effects), as well as binding of the reactant molecule, affecting the performance for hydrogen insertion.

**Table 1. Hydrogenation of unsaturated linear and cyclic C$_6$ hydrocarbons over β- and Y-graphenes.**

1-Hexene hydrogenation

$$1 \quad +H_2 \longrightarrow \quad 2 \qquad \text{Eq.(1)}$$

Catalyst	Time (h)	Conversion (%)	Selectivity (%)
Y	1.5	5	100
	3	10	100
	4	20	100
β	1.5	11.9	100
	3	29.8	100
	4	41	100

1-Hexyne hydrogenation

$$3 \quad +H_2 \longrightarrow \quad 4 \longrightarrow \quad 5 \qquad \text{Eq.(2)}$$

Catalyst	Time (h)	Conversion (%)	Selectivity (%)	
			4	5
Y	1.5	7	94.2	5.8
	3	13	87.8	12.2
	4	19	81.2	18.8
β	1.5	9.7	86.8	13.2
	3	22.4	83.9	16.1
	4	35.3	80.4	19.6

Cyclohexene hydrogenation

$$6 \quad +H_2 \longrightarrow \quad 7 \qquad \text{Eq.(3)}$$

Catalyst	Time (h)	Conversion (%)	Selectivity (%)
Y	1.5	22.6	100
	3	46	100
	4	48.9	100
β	1.5	26.8	100
	3	48.8	100
	4	64.1	100

Reaction conditions: 0.3 ml reactant : 0.3 ml heptane : 1 mg catalyst , 80 ˚C, 30 atm H$_2$, 800 rpm.

Table 2. Complex catalytic transformation of C8 and C10 linear alkenes and 1-Phenyl-1-hexyne over β- and Y-graphenes.

1-Octene hydrogenation

Catalyst	Time (h)	Conversion (%)	Selectivity (%) 9	10	11
Y	1.5	2	64.2	23.6	12.1
	3	15.5	57	28.6	14.4
	4	26.6	59.2	29.1	11.7
β	1.5	15.4 (11.8)	72.6 (86.9)	17.4 (6.5)	10 (6.6)
	3	31.5 (23.1)	75.2 (88.4)	16.1 (6.3)	8.7 (5.3)
	4	41 (36.1)	76.7 (90.7)	16.2 (4.6)	7 (4.7)

Reaction conditions: 0.3 ml reactant : 0.3 ml heptane : 1 mg catalyst (: 0.1ml methanol), 80 ˚C, 30 atm H_2, 800 rpm

1-Decene hydrogenation

Catalyst	Time (h)	Conversion (%)	Selectivity (%) 13	14	15	16
Y	1.5	9.3	26.4	25.1	0.8	47.7
	3	21.2	26.4	25.2	1.5	46.9
	4	28.6	27.0	25	1.25	46.8
β	1.5	38.2	72.4	12	0	15.6
	3	64.2	85.4	7.2	0	7.4
	4	80.3	87.7	5.5	0	6.8

Reaction conditions: 0.3 ml reactant : 0.3 ml heptane : 1 mg catalyst, 120 ˚C, 30 atm H_2, 800 rpm

1-Phenyl-1-hexyne hydrogenation

Catalyst	Time (h)	Conversion (%)	Selectivity (%) 18	19 (E)	20 (Z)
Y	1.5	17.2	40.3	49.3	10.4
	3	33.5	33.6	55.3	11.1
	4	43.2	31.2	56.2	12.6
β	1.5	23.8	43.2	47.1	9.7
	3	38.9	34.8	54.7	10.5
	4	49.6	32.7	55.8	11.5

Reaction conditions: 0.07 ml reactant : 0.53ml heptane : 1 mg catalyst, 100 ˚C, 30 atm H_2, 800 rpm

The reactions of 1-octene and 1-decene were even more appealing (Eq. 4 and 5 in table 2): the formation of the corresponding *n*-alkane was accompanied by intramolecular rearrangements including relocation of the double bond and branching of the linear chains. The skeletal isomerisation resulted for both linear terminal alkenes in selective production of 2-methyl-1-alkenes without the formation of other branched molecules (Table 2 and Figures S3 and S4). The double bond isomerisation selectively produced 2-ene (for 1-decene) and 4-ene (for 1-octene and 1-decene) linear alkenes. These reactions clearly demonstrate the bifunctional properties of the carbon materials as hydrogenating and acidic catalysts. In order to confirm the mechanism of the skeletal and double bond isomerisation of the *n*-alkenes via the formation of an intermediate on an acidic site, in other experiments 1-octene and 1-decene were mixed with methanol to block the potential "acid" sites of the catalysts (Table 2, values within backets for 1-octene hydrogenation). Indeed its addition enhanced both the conversion and the selectivity in *n*-octane with a corresponding decrease in the selectivity for 2-methyl-1-alkene. Based on all these results, it can be concluded that the catalysts promotes two concurrent mechanisms, one involving reduced graphene and the second with participation of the acidic functional groups on one-atom-thick graphene (Scheme 1).
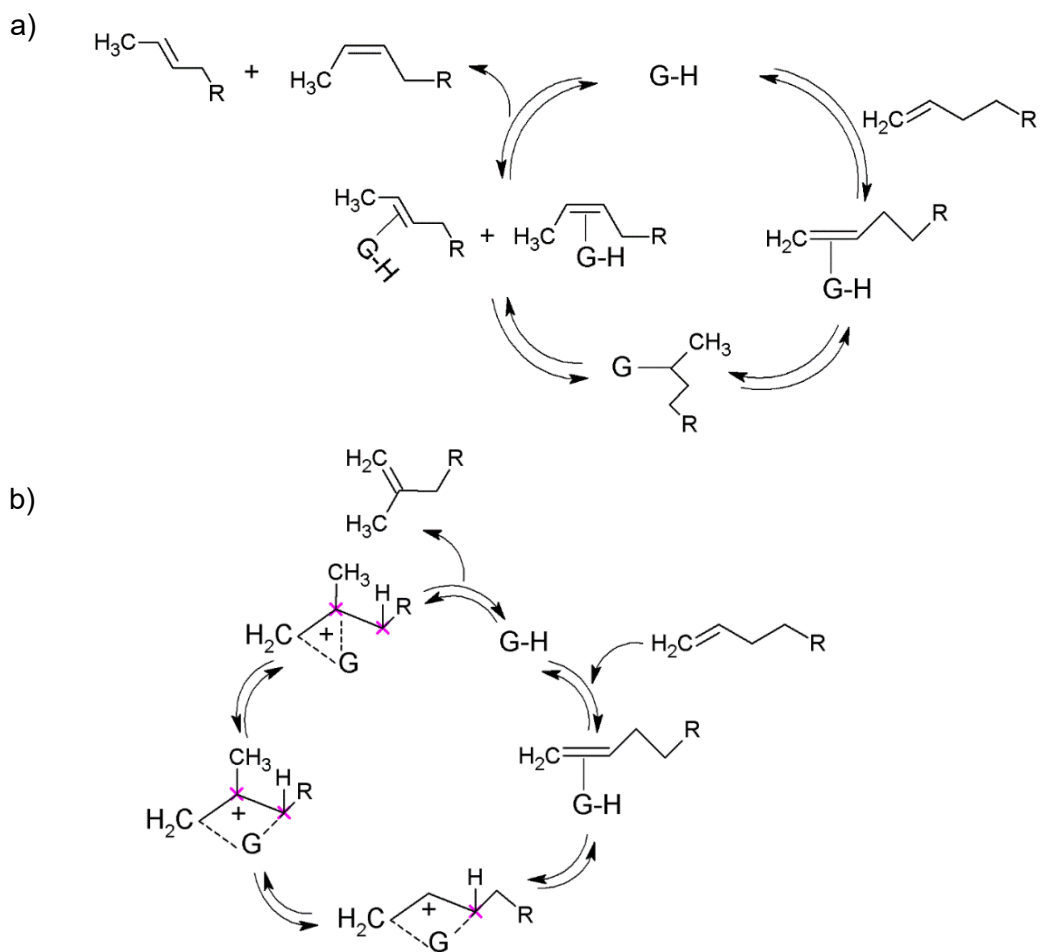
Scheme 1. *A) Double bond and B) skeletal isomerisation of 1-alkenes on G-catalysts.*

The hydrogenation of 1-phenyl-1-hexyne (Table 2) was performed to further demonstrate the unique nature of both Y-graphene and β-graphene for achieving stereocontrol in a catalytic reaction. The reaction was able to stereo-differentiate between the production of phenyl-1-hexene into the (E)-1-phenyl-1-hexene and (Z)-1-phenyl-1-hexene diastereoisomers. While the conversion was slightly higher on β-graphene, the E/Z ratio was about 5 for both materials, indicating that the thermodynamically more stable E isomers are the major products.

Several additional reactions were carried out to analyse the stability and durability of β-graphene and Y-graphene. Recycling the catalysts four times showed no loss in activity or selectivity in the reaction of 1-octene and no polymerization was produced during these reactions. In another experiment, the reaction was performed first with 1-octene (Table S1) and then the reaction products were removed and 1-hexyne was reacted for another 1.5 h with high reproducibility of the conversion and selectivity. To highlight the exceptional catalytic properties of 3D-graphene materials, the activities of β-graphene and Y-graphene in the reaction

of 1-octene hydrogenation were compared with that of graphene and Y-zeolite under identical conditions, observing for graphene and Y zeolite negligible conversions of 1-octene (~1%), (Table S1).

Discussions

Characterization data confirms that the highly stable graphene layers are spatially structured into 3D objects resembling the channel system in the regular crystalline structure of zeolites with a specific surface area comparable to the theoretical surface area of graphene. β-graphene and Y-graphene overcome the limitations arising from $\pi - \pi$ stacking and strong van der Waals interactions between sheets of graphene,[27] limiting the accessibility of the surface sites and dramatically decreasing the surface area of conventional graphene. The three-dimensional channel system of open microporosity β-graphene and Y-graphene and large specific surface area of the carbon particles are also significant advantages over traditional carbon nanotubes with precluded diffusion for even very small reactant molecules. The regularity of the porous system of the 3D carbon materials with pore openings fitting the molecular size of a variety of hydrocarbon molecules is also a unique characteristic of β-graphene and Y-graphene that is not available in graphene foam[33] or crumpled graphene[34].

Previous studies[7] indicated that a single layer of one-atom-thick graphene enables the activation of hydrogen and a hydrocarbon molecule for catalytic hydrogenation of carbon–carbon multiple bonds in unsaturated hydrocarbons. However, the activation of hydrogen on a defect-free graphene basal plane is known to be hindered by energetically unfavourable buckling of the surrounding carbon atoms induced by sp^3 binding of an isolated hydrogen atom. This barrier is not present in β-graphene and Y-graphene, where both sites of the sp^2 surface are accessible for hydrogen and, moreover, the interaction with hydrogen becomes favoured with the sp^2 surface curvature appropriate for accommodation of the hydrogen atoms.[35] The mutual surface curvature of the zeolite templated 3D carbon materials and the presence of a population of unsaturated carbon atoms at the edges of the sp^2 sheet are favourable factors decreasing the activation energy of the interaction between hydrogen and the carbon surface.[20]

In conclusion, the curved surface of a one-atom-thick layer of 3D structure β-graphene and Y-graphene having accessible porosity through the channel system and the presence of unsaturated carbon atoms at the edges, together with a low concentration of oxygen-containing functional groups facilitate hydrogenation of carbon–carbon multiple bonds that are accompanied by intramolecular rearrangements for selective relocation of the double bond, branching of the hydrocarbon chains, and stereo-selective isomerisations.

Methods

Synthesis of β-graphene and Y-graphene

The beta (*BEA), (NH_4^+ form, Si/Al 11.3, Zeolyst Int., CP814B -25, Lot. No. 814B-25-1597-77) and faujasite (FAU), (H^+ form, Si/Al = 6, Zeolyst Int., CBV712, Lot. No. 712014001708) zeolites[36] were used as hard templates for the preparation of 3D graphene-like microporous carbons denoted as *β-graphene* and *Y-graphene*, respectively. Carbonization of the zeolites was performed using chemical vapour deposition with propylene as a carbon precursor, followed by dissolution of the zeolite framework with HF and HCl acids. 1 g of the zeolite was placed in a quartz reactor, activated at 750 °C for 1 h at a heating rate of 3 °C min^{-1} under a stream of helium, carbonised in a propylene stream (5 vol % in He) for 2 h at 750 °C, then the propylene stream was switched to a stream of helium and the temperature was increased to 900 °C for 3 h at a heating rate of 3 °C min^{-1}. The zeolite was removed from the carbon/zeolite composite by leaching using a large excess of aqueous solutions of hydrofluoric and hydrochloric acids (the zeolite/carbon composite was stirred in a beaker with 350 ml 5 wt % HF solution at RT for 5 h, then with 50 ml 42 wt % HF solution for 1 h, and finally with 30 ml 37 wt % HCl solution for 1 h). The resulting nanocarbon sample was isolated by repeated centrifugations and washing with a large volume of water and filtration. The obtained material was dried in the air at 120 °C for 12 h. The employed procedure guaranteed quantitative removal of the zeolite template from the carbon materials.

The graphene (from pyrolysis of alginic acid at 900 oC under argon and subsequent exfoliation), Graphene oxide (Graphene oxide, 15-20 sheets, Lot. No. MKBW7125V), few-layer graphene (Graphene nanoplatelets, Lot. No. MKBX9558V) and graphite (Graphite, Lot. No. MKBV3964V) supplied by the Sigma-Aldrich Chemistry were used as standards for comparing the structural and catalytic properties.

Structural analysis

The X-ray powder diffraction (XRD) patterns were obtained using a Bruker AXSD8 Advance diffractometer with CuKα radiation in the Bragg–Brentano geometry and a position-sensitive detector (Våntec-1) in the 5-90° 2θ range.

The porosity of the carbons was determined by analysis of the adsorption isotherms of nitrogen at the boiling point of liquid nitrogen (77 K). Before the adsorption experiment, the samples were outgassed at 240 °C for at least 24 hours to ensure complete cleaning of the surface. The experiments were carried out using an ASAP2010 apparatus (Micromeritics). Because of the complex character of the sample porosity, namely the presence of both micropores and mesopores leading to the H4 types of hysteresis loops, a combination of procedures was used for analysis of the adsorption isotherms. The surface area was basically determined using the BET theory. The total pore volume and the external surface area (i.e., the surface area outside the pores) were determined by the Broekhoff-de Boer t-plot.

Using other standard isotherms, such as the Harkins-Jura or Halsey isotherms, provided practically the same data. Alternatively, the total pore volume was determined from the amount of nitrogen adsorbed at a relative pressure of about 0.99, converted to the volume of liquid nitrogen. Both data sets were in reasonable agreement. Finally, complex data on the sample porosity in a wide range encompassing both micropores and mesopores were obtained using the non-local DFT procedure based on several suitable models of carbonaceous sorbents.

High resolution transmission electron microscopy (HR-TEM), (JEOL JEM 3010) and scanning electron microscopy (SEM), (Jeol JSM-03) were used for imaging the morphology, shape and size of the zeolite, carbon/zeolite and carbon materials.

The Raman spectra were measured using a Labram HR spectrometer (Horiba Jobin-Yvon) interfaced to an Olympus BX-41 microscope with 50x objective using 488 nm (2.54 eV) laser excitation. The Raman spectrometer was calibrated by the F_{1g} line of Si at 520.5 cm^{-1}.

The XPS measurements were run using a ESCA 3 Mk II-VG spectrometer in a fixed transmission mode at passing energy of 20 eV (spectra measured at high resolution) and 50 eV (spectra measured at low resolution). The photoelectrons were excited by the Al K$\alpha_{1,2}$ emission line (hν = 1486.6 eV), where the detection angle of the photoelectrons θ was 45°. The vacuum during an experiment was of the order of $\approx 10^{-9}$ mbar.

Solid state NMR spectra were collected by magic angle spinning (MAS) using cross-polarization (CP) pulse sequence and the very fast (VF) approach. The ^{13}C CP/MAS and VF/MAS NMR spectra were measured on a Brucker Avance III HD 500 WB/US spectrometer (B$_0$ = 11.7 T) at Larmor frequency ν(^{13}C) = 125.783 MHz using either a double-resonance 4 mm or 2.5 mm MAS probe, respectively. The ^{13}C CP/MAS NMR spectra were acquired with spin lock time of 1750 μs, recycle delay of 2 s and 40960 scans. The spinning frequency of the rotor sample was 7 kHz. During acquisition, high-power dipolar decoupling (SPINAL 64) was used to eliminate strong heteronuclear dipolar couplings. The ^{13}C VF/MAS NMR experiments were recorded without a decoupling sequence using the spin-echo approach (π/2-(t_1)-π-aq.), where the t_1 delay was rotor synchronized (1 loop). All the VF/MAS NMR experiments were performed at a spinning frequency of 25 kHz[37] with a π/2 pulse length of 2.2 μs, recycle delay of 2 s and 38400 scans. The ^{13}C NMR isotropic chemical shifts were referenced to glycine as an external standard (low-field carbonyl signal at 176.03 ppm). All the samples were placed in ZrO$_2$ rotors, sealed with Kel-F caps and the NMR experiments were performed at laboratory temperature. The moderate frictional heating of the spinning samples was compensated by active cooling[38].

Thermogravimetric analysis coupled to differential scanning calorimetry (TG-DSC) analysis was performed on a Setaram TG-DSC 111 instrument. Two subsequent measurements were carried out on each carbon sample. The first measurement was performed in argon with a constant flow rate of 20 ml min^{-1} and the second measurement was performed in a mixture of oxygen and argon (20 vol % O$_2$

in Ar) at atmospheric pressure. In both cases, the samples were heated from 25 to 800 °C at a constant heating rate of 10 °C min^{-1}. The mass of the sample was ~5 mg and an empty Al_2O_3 crucible was used as a reference.

Catalytic tests

XXXX

Catalytic tests

GC-MS

1H and 13C MNR

Acknowledgments

References

(1)   Bonaccorso, F.; Colombo, L.; Yu, G.; Stoller, M.; Tozzini, V.; Ferrari, A. C.; Ruoff, R. S.; Pellegrini, V. *Science* **2015**, *347*.

(2)   Stankovich, S.; Dikin, D. A.; Dommett, G. H. B.; Kohlhaas, K. M.; Zimney, E. J.; Stach, E. A.; Piner, R. D.; Nguyen, S. T.; Ruoff, R. S. *Nature* **2006**, *442*, 282.

(3)   Geim, A. K.; Novoselov, K. S. *Nat. Mater.* **2007**, *6*, 183.

(4)   Castro Neto, A. H.; Guinea, F.; Peres, N. M. R.; Novoselov, K. S.; Geim, A. K. *Rev. Mod. Phys.* **2009**, *81*, 109.

(5)   Geim, A. K. *Science* **2009**, *324*, 1530.

(6)   Novoselov, K. S.; Falko, V. I.; Colombo, L.; Gellert, P. R.; Schwab, M. G.; Kim, K. *Nature* **2012**, *490*, 192.

(7)   Primo, A.; Neatu, F.; Florea, M.; Parvulescu, V.; Garcia, H. *Nat. Commun.* **2014**, *5*.

(8)   Primo, A.; Esteve-Adell, I.; Blandez, J. F.; Dhakshinamoorthy, A.; Álvaro, M.; Candu, N.; Coman, S. M.; Parvulescu, V. I.; Garćia, H. *Nat. Commun.* **2015**, *6*.

(9)   Primo, A.; Puche, M.; Pavel, O. D.; Cojocaru, B.; Tirsoaga, A.; Parvulescu, V.; García, H. *Chemical Communications* **2016**, *52*, 1839.

(10)   Gao, Y.; Ma, D.; Wang, C.; Guan, J.; Bao, X. *Chemical Communications* **2011**, *47*, 2432.

(11)   Wei, Z.; Hou, Y.; Yang, Y.; Liu, Y. *Curr. Org. Chem.* **2016**, *20*, 2055.

(12)   Serp, P.; Corrias, M.; Kalck, P. *Applied Catalysis A: General* **2003**, *253*, 337.

(13)   Kim, K.; Lee, T.; Kwon, Y.; Seo, Y.; Song, J.; Park, J. K.; Lee, H.; Park, J. Y.; Ihee, H.; Cho, S. J.; Ryoo, R. *Nature* **2016**, *535*, 131.

(14)   Xia, Y.; Yang, Z.; Mokaya, R. *Nanoscale* **2010**, *2*, 639.

(15)   Inagaki, M.; Orikasa, H.; Morishita, T. *RSC Advances* **2011**, *1*, 1620.

(16)   Kyotani, T.; Nagai, T.; Inoue, S.; Tomita, A. *Chemistry of Materials* **1997**, *9*, 609.

(17)   Itoi, H.; Nishihara, H.; Kogure, T.; Kyotani, T. *Journal of the American Chemical Society* **2011**, *133*, 1165.

(18)   Nishihara, H.; Kyotani, T. *Advanced Materials* **2012**, *24*, 4473.

(19)   Kajdos, A.; Kvit, A.; Jones, F.; Jagiello, J.; Yushin, G. *Journal of the American Chemical Society* **2010**, *132*, 3252.

(20)   Yang, Z.; Xia, Y.; Mokaya, R. *Journal of the American Chemical Society* **2007**, *129*, 1673.

(21)   Masika, E.; Mokaya, R. *Energy and Environmental Science* **2014**, *7*, 427.

(22)   Antoniou, M. K.; Diamanti, E. K.; Enotiadis, A.; Policicchio, A.; Dimos, K.; Ciuchi, F.; Maccallini, E.; Gournis, D.; Agostino, R. G. *Microporous and Mesoporous Materials* **2014**, *188*, 16.

(23)   Jiang, C.; Hara, K.; Namba, K.; Kobayashi, H.; Ittisanronnachai, S.; Nishihara, H.; Kyotani, T.; Fukuoka, A. *Chemistry Letters* **2014**, *43*, 1794.

(24)   Xia, Y.; Mokaya, R.; Walker, G. S.; Zhu, Y. *Advanced Energy Materials* **2011**, *1*, 678.

(25)   Higgins, J. B.; Lapierre, R. B.; Schlenker, J. L.; Rohrman, A. C.; Wood, J. D.; Kerr, G. T.; Rohrbaugh, W. J. *Zeolites* **1988**, *8*, 446.

(26)   Treacy, M. M. J.; Newsam, J. M. *Nature* **1988**, *332*, 249.

(27)   Jiang, L.; Fan, Z. *Nanoscale* **2014**, *6*, 1922.

(28)   Ferrari, A. C. *Solid State Commun* **2007**, *143*, 47.

(29)   Ferrari, A. C.; Meyer, J. C.; Scardaci, V.; Casiraghi, C.; Lazzeri, M.; Mauri, F.; Piscanec, S.; Jiang, D.; Novoselov, K. S.; Roth, S.; Geim, A. K. *Phys Rev Lett* **2006**, *97*.

(30)   Dreyer, D. R.; Park, S.; Bielawski, C. W.; Ruoff, R. S. *Chemical Society Reviews* **2010**, *39*, 228.

(31)   Sen, B.; Vannice, M. A. *Journal of Catalysis* **1991**, *130*, 9.

(32)   Gruber, H. L. *Journal of Physical Chemistry* **1962**, *66*, 48.

(33)   Chen, Z.; Ren, W.; Gao, L.; Liu, B.; Pei, S.; Cheng, H. M. *Nat. Mater.* **2011**, *10*, 424.

(34)   Zang, J.; Ryu, S.; Pugno, N.; Wang, Q.; Tu, Q.; Buehler, M. J.; Zhao, X. *Nat. Mater.* **2013**, *12*, 321.

(35)   Stojkovic, D.; Zhang, P.; Lammert, P. E.; Crespi, V. H. *Physical Review B* **2003**, *68*, 195406.

(36)   Sazama, P.; Kaucky, D.; Moravkova, J.; Pilar, R.; Klein, P.; Pastvova, J.; Tabor, E.; Sklenak, S.; Jakubec, I.; Mokrzycki, L. *Applied Catalysis A: General* **2017**, *533*, 28.

(37)   Shaibat, M. A.; Casabianca, L. B.; Wickramasinghe, N. P.; Guggenheim, S.; de Dios, A. C.; Ishii, Y. *Journal of the American Chemical Society* **2007**, *129*, 10968.

(38)   Brus, J. *Solid State Nuclear Magnetic Resonance* **2000**, *16*, 151.